PERGAMON

Chaos, Solitons and Fractals 14 (2002) 901–916

CHAOS
SOLITONS & FRACTALS

www.elsevier.com/locate/chaos

Power laws and fractal behavior in nuclear stability, atomic weights and molecular weights

V. Paar *, N. Pavin, A. Rubčić, J. Rubčić

Faculty of Science, Department of Physics, University of Zagreb, Bijenička 32, 10000 Zagreb, Croatia

Accepted 15 January 2002

Abstract

A power law is introduced for the description of the line of stability of atomic nuclei, and for the description of atomic weights and molecular weights. The power law for the line of stability is compared with the semi-empirical formula of the liquid drop model. It is shown that the power law corresponds to a reduction of neutron excess in superheavy nuclei with respect to the semi-microscopic formula. Some fractal features of the nuclear valley of stability and of the isotopic abundance set of molecules are shown and the corresponding fractal dimensions are determined. With respect to the problem of truncating fractals of natural objects, it is shown that a simple mathematical model of an extended map on an annulus provides a similar type of truncated fractals. It is argued that the origin of the observed fractal property of nuclei, atoms and molecules lies in the basic fractal nature of quantum mechanics.

1. Introduction

The concept of fractal geometry, closely linked to scale invariance, provides a framework for the analysis of natural phenomena in various scientific domains [1–7]. Many investigations have implemented fractal ideas to study various forms in nature. Fractal structures have been found on different length scales, from astronomic to microscopic scales. Examples include clusters of galaxies [1,8,9], distribution of earthquakes [10], the structure of coastlines and rivers [11], cracks in sedimentary rocks [12], protein surfaces [13], etc. Moreover, the occurrence of fractals is not limited to structures in real space. In many cases fractal properties are "hidden" and can only be perceived if data are studied as a function of time or mapped in some special way [6]. For example, in some cases the length scale in the fractal definition is replaced by a time scale, for example, in the time series of heartbeat [6,14], in electric current through ion channels in a cell membrane [15], in reactions of heterogeneous chemistry [2], in the basal metabolic rate in biological organisms [16].

It is well known that a power law is often connected with an underlying fractal geometry of the system [3,4]. Examples of such relations are the power law dependence of the basal metabolic rate on the mass of mammals and the fractal structure of organs [16], the power law distribution of a drainage-basin area and the fractal dimension of a river network [11], the power law in X-ray scattering from a rat lens nucleus which may be evidence of fractal structures in the lens [17], etc.

Power laws have been found also in cases without being related to an underlying fractal geometry. For example, a power law dependence on molecular weights was found experimentally for the interactions between polyethylene oxide layers adsorbed to glass surfaces [18], for stretching ridges in a crumpled elastic sheet [19], etc.

* Corresponding author. Tel.: +385-1-3364272; fax: +385-1-4680336.
E-mail address: paar@hazu.hr (V. Paar).

0960-0779/02/$ - see front matter
PII: S0960-0779(02)00032-2

In this paper we apply ideas from fractal geometry to the valley of stability of atomic nuclei and to atomic and molecular weights. In Section 2 we introduce the power law for the description of the line of nuclear stability and consider its extension to super-heavy nuclei. The relation of the power law to the well-known semi-microscopic formula is discussed. In Section 3 the fractal nature of the valley of stability in the N,Z-chart of nuclides is investigated. In Section 4 we introduce the power law for description of the systematic of atomic weights. In Section 5 we introduce the power law for the description of molecular weights and exemplify it for a random selection of molecules. In Section 6 the fractal nature in the isotopic composition of chemical compounds is analyzed. In Section 7 we present a model for a truncated fractal, which is a feature characterizing all natural fractals, including hidden fractals studied in this paper.

2. Power law for the nuclear valley of stability

The problem of stability of atomic nuclei has for a long time received considerable attention in terms of modeling in nuclear dynamics [20–30]. Recent success in the synthesis of new super-heavy nuclei has invigorated this interest [31–34].

A broad variation of the region of stable atomic nuclei is largely determined by competition between the symmetry and Coulomb energy [22]. Trends of nuclear stability are shown in the N, Z-chart of nuclides (Fig. 1). (The nucleus with Z protons and N neutrons has the mass number $A = Z + N$.) Solid boxes represent stable nuclei plotted in dependence on the mass number N and atomic number Z, forming the well-known "valley of stability". The corresponding pattern of the valley of stability appears in the A, Z-chart of nuclides.

A line through the valley of stability in the nuclear chart is known as the line of stability. The line of stability obtained by taking for each atomic number Z the stable nucleus of the isotope with largest relative abundance is displayed in Fig. 2 (open circles). The naturally occurring long-lived elements are also included. In addition, the nucleus with $Z = 114$, $A = 298$, predicted theoretically to be the most stable super-heavy isotope [24–30], is displayed ($\times$).

For light nuclei, where the symmetry energy term is dominant, the line of stability approximately follows the line $N = Z$, i.e., $Z = A/2$. With increasing mass number the line of stability deviates from the straight line as the Coulomb energy term becomes increasingly important, causing heavier stable nuclei to have an increased excess of neutrons over protons. The general trend of the line of stability follows from the semi-empirical mass formula by minimizing the total nuclear mass [22]:

$$A - 0.006A^{5/3} = 2Z. \tag{1}$$

More specifically, this formula corresponds to the β-stable species, i.e., to the valley of β-stability [22]. This should be kept in mind when extrapolating to super-heavy nuclei, where the β-stable isotopes of longest lifetime lie on the line of β-stability.

The prediction of the semi-empirical formula (1) for the line of stability is displayed in Fig. 2 (dotted line).

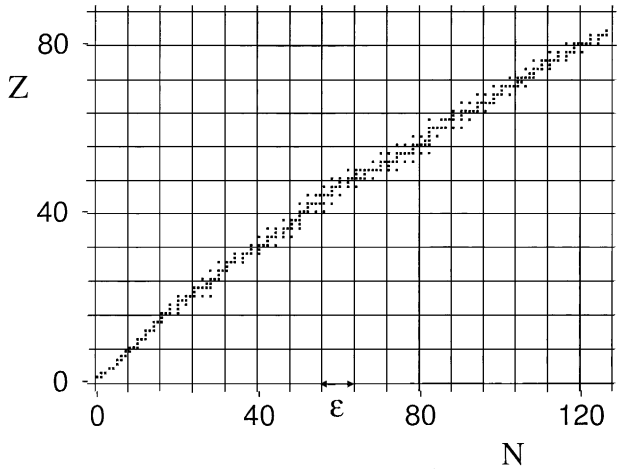

Fig. 1. Valley of stability in the N,Z-chart of nuclides. Solid boxes: stable nuclei and long-lived naturally occurring β-stable nuclei in dependence on the neutron number N and the atomic number Z.

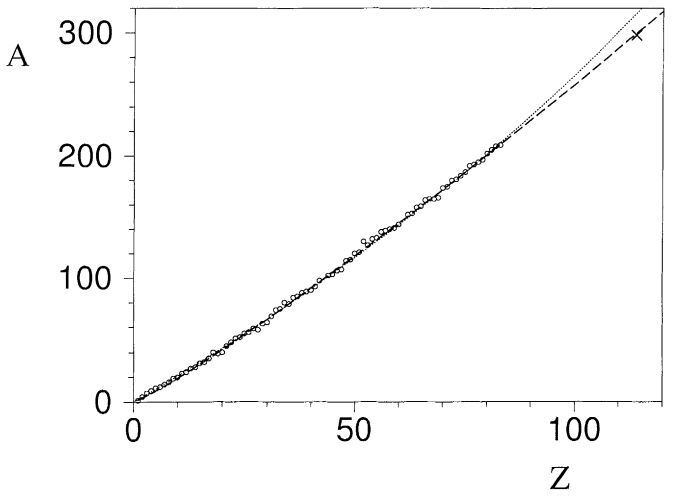

Fig. 2. A, Z-plot of the power law (2) (dashed line) fitted to nuclei on the line of stability (open circles). For comparison, prediction of the semi-empirical mass formula (1) is displayed too (dotted line). In addition to stable nuclei, the position of super-heavy doubly closed shell nucleus $^{298}114$ is also shown ($\times$) (not included in the fit).

Here we propose another approach to the problem of stability of atomic nuclei, related to identifying basic features in underlying dynamics, which give rise to the structure of atomic nuclei. In this connection we note that the role of fractal geometry in quantum physics and quark dynamics was recently discussed [35]. It was pointed out that the fractal geometry, which shows up in particular observables, is generated by the dynamics of the quantum system, the first example of fractal geometry in quantum systems showing up in the self-similarity of paths of the Feynman path integral. It was shown that velocity-dependent interactions, which appear in the theory of nuclear matter, lead to a noninteger dimension and that the fractal dimension appears for free the fermion propagator which is relevant for the geometry of quark propagation in quantum chromodynamics [35]. On this basis one may argue for the appearance of scale invariance at the level of bulk properties of atomic nuclei.

On the basis of this argument and of the observation that the shape of the valley of stability in nuclear chart resembles a fractal-like pattern, we suggest to introduce a scale invariant power law for the line of stability:

$$A = \alpha Z^{\beta}. \tag{2}$$

A fit of the power law (2) to data for the naturally occurring nuclei forming a line of stability gives:

$$\alpha = 1.47 \pm 0.02, \tag{3}$$

$$\beta = 1.123 \pm 0.005. \tag{4}$$

The fitted curve of the power law is displayed in Fig. 2 (dashed line). A rather good quality of fit is obtained. The χ^2-value given by

$$\chi^2 = \sum_i \frac{1}{N} [Z_i - Z_i(A_i)]^2 \tag{5}$$

with summation over $N = 81$ stable nuclei and using the power law formula (2) with parameters (3), (4) for $Z_i(A_i)$ yield $\chi^2 = 0.44$. This is a comparable and slightly better fit than the fit obtained by using the semi-empirical mass formula (1) where $\chi^2 = 0.69$. Even if we modify the semi-microscopic formula (1) by introducing free parameters a and $b : A - aA^{5/3} = bZ$, the power law formula still provides a comparable and a slightly better fit. In any case, we can conclude that the fits of the power law formula (2) and of the semi-empirical mass formula (1) to the line of stability are comparable.

If we extrapolate the graphs corresponding to both formulas towards heavier nuclei, above the naturally occurring nuclei, it is observed that the graph corresponding to the semi-empirical mass formula (1) (dotted line) is more concave than the graph corresponding to the power law (2) (dashed line). Thus, the difference between predictions of the two formulas increases with increasing mass of super-heavy nuclei.

Most of the theoretical calculations predicted the next double shell closure beyond ^{208}Pb at the proton number $Z = 114$ and the neutron number $N = 184$ [24–30], which appears in accordance with recent experiments [31–34]. This nucleus is expected to have a very long lifetime, lying on the extrapolation of the line of stability. The position of this nucleus is shown by $\times$ in Fig. 2. As can be seen, it lies somewhat closer to the graph predicted by the power law (2) than to the graph predicted by the semi-empirical formula (1).

We may conclude that for naturally occurring nuclei the power law formula (2) is in good accordance with the semi-empirical formula (1), i.e., that the underlying fractal nature leads to a similar bulk pattern as the dynamics of the semi-empirical model. Only if extended towards super-heavy nuclei, the power law formula (2) starts to show a systematic difference with respect to the semi-empirical formula, giving a somewhat slower increase of the neutron excess with Z, than predicted by the semi-empirical formula (1). Thus the tendency toward stability for $N = Z$ for super-heavy nuclei is more pronounced for the power law formula (2) than for the semi-empirical formula (1). This could be accounted for in the semi-empirical formula (1) by slightly enhancing the symmetry energy term with increasing mass for super-heavy nuclei, i.e., by increasing the strength of symmetry energy for super-heavy nuclei over its standard value of $b_{\mathrm{sym}} = 50$ MeV in the semi-empirical mass formula, for example, by introducing a slight increase of b_{sym} with A as $b_{\mathrm{sym}} = 50(1 + \varepsilon A^{\eta})$ MeV, with ε being a small parameter.

On the other hand, one should note that the expression $-\frac{1}{2}b_{\mathrm{sym}}[\{(N-Z)^2\}/A]$ for the symmetry energy in the semi-empirical mass formula represents only a leading effect for small values of $(N-Z)/A$, while there is no corresponding approximation in the power law formula. It was pointed out [22] that more exact tests of the semi-empirical mass formula are encountered when one tries to treat nuclei much heavier than those naturally occurring. For this purpose additional terms in the semi-empirical formula may be required, describing, for example, a dependence of the surface energy and of the average nuclear density on the charge symmetry parameter, $N - Z$ [22]. These additional terms could increase the tendency in favor of $N = Z$ for the line of stability, thus bringing the prediction of modified semi-empirical formula closer to the prediction of the power law formula for super-heavy nuclei.

3. Fractal geometry associated with the nuclear valley of stability

In Section 2 we have found a power law for stable nuclei, describing the line of nuclear stability. As to the origin of this power law the underlying quantum-mechanical fractal nature was pointed out. Let us now look for some specific fractal-like features which appear for stable nuclei, in analogy to some previously investigated cases of natural objects showing that phenomenological power laws are associated with some underlying fractal pattern [1–7]. It will be shown here that fractal geometry can be seen in the shape of the valley of stability in the nuclear chart [22,36].

The shape of the valley of stability can be considered as being determined by a boundary between the regions of β^-- and β^+-radioactive nuclei in the chart of nuclides. Now we calculate the fractal dimension of the valley of stability in the N, Z-chart of nuclides employing the box-counting method, which has a wide range of applications [4]. Here we use the box-counting method for a ''granular'' structure provided by the N, Z-sites (boxes) in the chart of nuclides.

Usually to determine fractal dimension of an object in nature, the photographs of the object are digitized using a grid of pixels [37]. The fractal dimension of the digitized pattern is then obtained using the box-counting method. A similar approach, but having a much smaller number of pixels, is adopted in our study of the chart of nuclides. We assign one pixel to each site in the chart of nuclides corresponding to a stable nucleus. Then the box-counting method is applied to pixels, which correspond to the valley of stability. The chart is overlaid with a grid of square boxes of size $\varepsilon = \Delta Z = \Delta A$. Grids of different sizes are used. The number of nonempty boxes N_i of size ε_i is plotted on the log–log diagram as a function of ε_i (Fig. 3). An approximate straight-line correlation is obtained in the interval from $\varepsilon = 2$ to $\varepsilon = 18$. We note that this range of grid sizes is in accordance with the general requirement that the finest grid size must be larger than the pixel size and that the number of nonempty boxes has to be sizeable [5]. The slope of this line gives the fractal dimension d_{f} of the valley of stability in the N, Z-chart:

$$d_{\mathrm{f}} = 1.19 \pm 0.01. \tag{6}$$

As seen from Fig. 3, the log–log plot for the chart of stable nuclei significantly differs from the line which would correspond to a nonfractal distribution (i.e., of dimension 1).

Thus, the valley of stability in the nuclear chart appears as a line-area hybrid, a fractal object over roughly a decade in the length scale ε. For comparison, we note that this range, although limited, is within the range of fractals occurring in natural objects; an analysis of a wide collection of physical systems showed that the range of appropriate scaling properties for declared fractal objects in nature is centered around one (more precisely, 1.3) orders of magnitude [38].

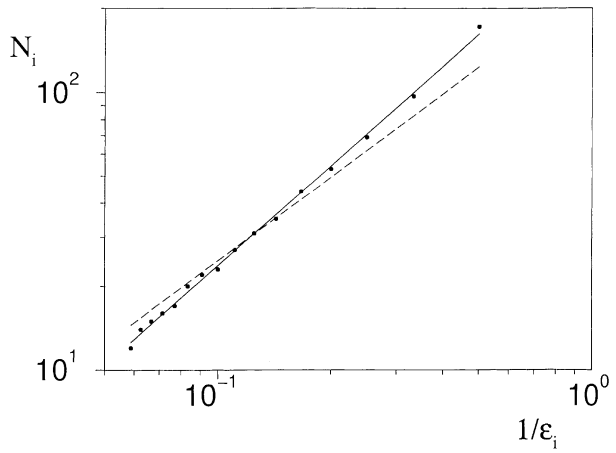

Fig. 3. Log–log plot for the number of nonempty boxes vs. $1/\varepsilon$ (ε is the size of a grid box) covering the N, Z-chart of nuclides. Straight line: a fit through the points calculated for different values of the box size ε. Dashed line: straight line which would correspond to $d_f = 1$.

4. Power law for atomic weights of chemical elements

Concept of atomic weights is fundamental to chemistry. The atomic weight of a naturally occurring chemical element is the average of the corresponding isotope weights, weighted to take into account relative isotopic abundances [39–41]. The problem to determine atomic weights has occupied the attention of chemists for a long time. Now we address the question of a possible mathematical formula giving an approximate expression for atomic weights in dependence on the atomic number Z. In the framework of the fractal approach, employed in Section 2 for the nuclear line of stability, we introduce a power law formula giving an approximate expression for atomic weights A_r of stable chemical elements in dependence on atomic number Z:

$$A_r = \alpha_c \, Z^{\beta_c} \tag{7}$$

A fit of the power law (7) to the data of atomic weights [39] gives the values of parameters in the power law:

$$\alpha_c = 1.44 \pm 0.02, \tag{8}$$

$$\beta_c = 1.120 \pm 0.004. \tag{9}$$

The fitted curve is displayed in Fig. 4 (solid line). The corresponding χ^2-value is $\chi^2 = \sum_i (1/N)[A_{ri} - A_r(Z_i)]^2 = 0.28$, where A_{ri} denotes the standard atomic weight of a chemical element with atomic number Z_i, and $A_r(Z_i)$ denotes the value of atomic weight calculated using the atomic power law (7). The summation is extended over $N = 81$ stable chemical elements.

In addition to stable chemical elements (open circles), we display an extrapolation of the atomic power law (7) using the parametrization (8), (9) to atomic weights of unstable heavy and super-heavy elements for which the most stable isotopes are known (open triangles), and to the region of expected island of stability at $Z = 114$ [34].

The atomic power law (7) provides a good phenomenological description of atomic weights. On the other hand, the power law captures something about the internal structure of the object. We note that the semi-empirical formula (1) approximately corresponds to the atomic power law (7). This is seen from the fit of both formulas to the stable chemical elements: the χ^2-value in the log–log plot for a fit of the semi-empirical formula is $\chi^2 = 0.007$, while the fit of the atomic power law (1) gives $\chi^2 = 0.004$. One might further argue whether the somewhat smaller χ^2-value for the power law formula is significant.

In conclusion, we have introduced the power law for atomic weights A_r in dependence on the atomic number Z. A fit of this formula to the data for A_r leads to a power law exponent, which is practically the same as the value corresponding to the nuclear line of stability. Consequences of this expression in the astrophysical context are discussed in [43].

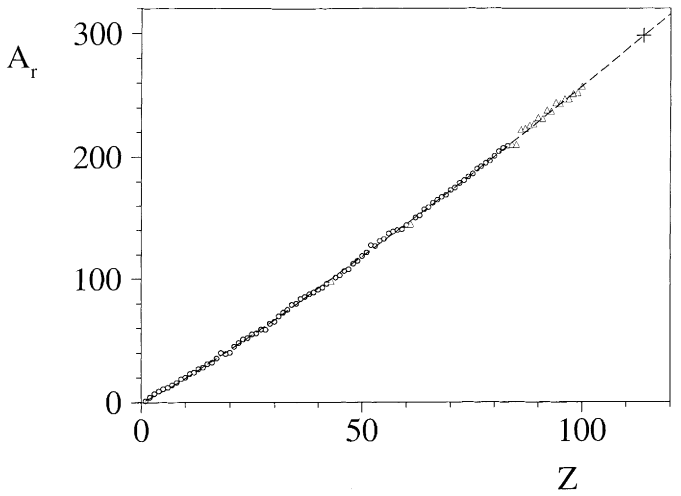

Fig. 4. A_r, Z-plot of the power law (7) (solid line) fitted to atomic weights of stable chemical elements (open circles). Open triangles: atomic weights of naturally occurring radioactive elements and of super-heavy elements up to $Z = 100$ defined according to [39,41] ; $\times$: the expected $Z = 114$ super-heavy element.

5. Power law for molecular weights of chemical compounds

There exist a number of applications of the fractal-geometry concept to chemistry. Let us name a few examples. Fractals have found a wide range of applications in the studies of colloidal aggregation phenomena [44–46]. The fractal geometry of small particle aggregates plays important role in their physical behavior, including kinetics of the aggregation process [47,48]. Fractal geometry was studied in the context of fractal molecules, self-similar to their branches [49]. Sol–gel transition, structure and the properties of critical gels in polymer systems were investigated and a power law for dependence of the static properties of critical gels was found [50]. Cluster structure and the arrangement of clusters in the diffusion-limited cluster-cluster aggregation simulation model of colloidal aggregation were studied, with individual clusters having a fractal structure [51].

A fractal reaction dimension was employed in dissolution studies of powder substances with a given particle size distribution [52]. A power law dependence was found for variation of the screening length with concentration and of the squared radius of a labeled chain with concentration in a semi-dilute solution in a good solvent [53]. Theoretical simulations have demonstrated that screening, trapping, selective reactivity, roughening and smoothing, when applied to fractal or smooth objects, result in effective structures which are still describable in terms of the scaling fractal exponent [54]. There are a large number of recent applications of the fractal concept to chemistry, with many examples of fractals related to the corresponding power laws (for example, [55–65]).

Having in mind that the atomic weights of naturally occurring chemical elements are averages of the corresponding isotope weights, weighted to take into account relative abundances of isotopes, the molecular weight of each chemical compound can be considered as a weighted average of isotopic weights of all isotopic configurations (combinations of nuclides) corresponding to the chemical formula of the compound. In this paper we address the following question: How far can one go back to the fundamental chemical level to apply the fractal concept, and in particular, can one trace the fingerprints of fractal geometry in molecular weights? Here we introduce phenomenologically the power law for molecular weights in the framework of fractal ideas of Mandelbrot and discuss its origin.

In Section 4 we have shown that the scale invariant power law for atomic weights (7) provides a good description of the data.

Let us consider a molecule:

$$(E_1)_{n_1}(E_2)_{n_2},\ldots,(E_s)_{n_s} \tag{10}$$

containing n_i atoms of chemical element E_i with atomic number Z_i ($i = 1, 2, \ldots, s$), and $\sum_i n_i = n$. Using the atomic power law (7), we can express the molecular weight of a molecule (10) as

$$M_r = \alpha_c \sum_i n_i Z_i^{\beta_c}. \tag{11}$$

Similarly as in [66] we introduce the molecular power law:

$$M_r = \alpha Z_{\text{eff}}^{\beta}, \tag{12}$$

where Z_{eff} denotes a parameter characterizing the molecule (10), which has to be determined.

On the basis of comparison of Eq. (11) and the power law (12) the effective molecular number Z_{eff} is defined by

$$Z_{\text{eff}} = \left(\sum_i n_i Z_i^{\beta_c} \right)^{1/\beta_c}, \tag{13}$$

where $\beta = \beta_c$ is used. Let us take $\beta_c = 1.120$ from the fit of Eq. (7) to the data of atomic weights. (We note that because of the power law functions in Eqs. (11) and (12) similar results are obtained by considering a more general relation $\beta = k\beta_c$, with k being an arbitrary coefficient of proportionality.)

We note that for the value $\beta_c = 1$, Eq. (13) reduces to the sum of atomic numbers of all atoms contained in the molecule, $Z_{\text{tot}} = \sum_i n_i Z_i$.

For some molecules the values of Z_{eff} and Z_{tot} differ sizably, up to $\approx 50\%$. For example, for the molecule $H_5BW_{12}O_{40} \cdot 30H_2O$ there is $Z_{\text{eff}} = 995$, $Z_{\text{tot}} = 1518$.

Let us now display the log–log plot for molecular weights M_r in dependence on Z_{eff} for a random set of 381 molecules. This set was formed by selecting 381 molecules from the list of inorganic molecules in [67]. Molecules were selected by using the logistic equation with the control parameter of 4 as the generator of random numbers, used to select ordering numbers of molecules from the list of molecules in [67] (Table 1).

For each chemical compound the corresponding data point is displayed (open circles in Fig. 5).

In the next step, a fit of the power law (12) to these data points is performed (solid line in Fig. 5). Very good fit was obtained with:

$$\alpha = 1.55 \pm 0.03, \tag{14}$$

$$\beta = 1.114 \pm 0.002, \tag{15}$$

Table 1
Randomly selected ordering numbers of molecules from the list of molecules in [67]. The logistic equation at $r = 4$ was used as the random number generator

a17, a20, a23, a24, a28, a35, a40, a44, a47, a78, a101, a112, a134, a137, a138, a140, a142, a143, a147, a169, a186, a197, a217, a221, a227, a237, a251, a285, a286, b4, b7, b22, b31, b54, b67, b74, b98, b110, b112, b157, b164, b168, b179, b211, b213, b215, c4, c19, c26, c44, c48, c51, c67, c83, c118, c131, c132, c135, c148, c158, c165, c169, c202, c203, c213, c232, c235, c236, c239, c250, c259, c260, c286, c290, c294, c316, c324, c336, c362, c367, c386, c394, c396, c399, c403, c422, c451, c454, c469, c473, c477, c479, c486, c504, c509, c512, c524, c532, c547, c551, c558, c571, c576, c586, c594, c598, c615, c621, c625, c630, c631, c634, c646, c655, c664, d11, d16, e10, e18, e19, e21, f11, g14, g16, g22, g23, g32, g35, g37, g42, g56, g62, g71, g72, g78, g93, g99, h9, h21, h31, h46, h66, i19, i24, i26, i27, i36, i49, i63, i70, i82, i83, i93, i107, i108, i116, i121, i134, i139, i155, i156, i157, i163, l2, l7, l34, l47, l60, l73, l74, l87, l88, l98, l104, l129, l130, l135, l137, l138, l151, l168, l169, l174, l175, l196, l220, m34, m36, m56, m64, m72, m82, m88, m133, m141, m155, m196, m211, m216, m223, m257, m258, m264, m289, m299, m301, n18, n27, n42, n44, n56, n82, n88, n108, n126, n139, n140, o2, o20, p11, p13, p37, p56, p74, p75, p80, p136, p141, p176, p190, p195, p204, p230, p255, p293, p302, p314, p316, p325, p338, p348, p356, p358, p364, p369, p374, p379, p383, p387, p393, p409, p415, p458, p467, p475, p488, p491, p501, p508, p527, p532, r2, r25, r27, r31, r47, r60, r70, r79, r84, r91, r116, r118, r120, s3, s18, s23, s45, s46, s54, s55, s57, s75, s79, s105, s106, s110, s117, s132, s146, s155, s171, s172, s182, s198, s226, s229, s237, s262, s275, s317, s341, s361, s363, s375, s381, s392, s396, s419, s437, s443, s457, s482, s499, s507, s510, s515, s520, s540, s548, s556, t5, t8, t19, t25, t39, t45, t51, t66, t73, t90, t120, t121, t128, t136, t150, t161, t169, t172, t188, t193, t208, t209, t251, t258, t268, t289, u15, u18, u20, u22, u23, v1, v2, v4, v16, v23, v32, y7, y9, y11, y19, y21, y22, y24, y27, y31, y35, z2, z7, z12, z19, z20, z32, z58, z75, z77, z81, z95, z97, z111

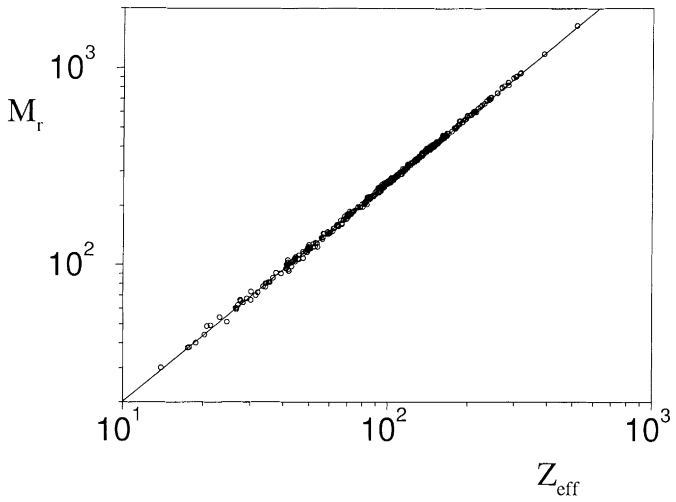

Fig. 5. Log–log M_r, Z_{eff}-plot of data points for molecular weights of 381 randomly selected inorganic compounds from [67] in dependence on the effective molecular number Z_{eff} (open circles). The straight line presents a fit of the power law (Eq. (12)) to data.

indicating applicability of the power law (12) to molecular weights. Similar values were obtained in the previous fit for a set of 180 randomly chosen molecules [66].

To gain a better insight into the quality of the power law (12) in fitting molecular data in the M_r vs. Z_{eff} diagram for the set of molecules from Table 1, we have considered, for comparison, a diagram displaying M_r in dependence on the total proton number Z_{tot} (Fig. 6). The scattering of data points in the M_r vs. Z_{tot} diagram in Fig. 6 is much larger (the χ^2-value is 15 times larger) than in the M_r vs. Z_{eff} diagram in Fig. 5. (Here, $\chi^2 = \frac{1}{n}\sum_i [\ln M_r(i) - (\ln\alpha + \beta \ln Z_{\text{eff}}(i))]^2$.)

In order to test the consistency of the fitted values (14), (15) let us consider an alternative fitting procedure. Instead of using the fitted value of β_c to calculate Z_{eff} for construction of data points in the M_r vs. Z_{eff} diagram, let us start with a set of uniformly distributed initial values of β_c. For each initial value of β_c we calculate the corresponding Z_{eff}-value using Eq. (13), and the corresponding M_r vs. Z_{eff} diagram is constructed. Then, the fit of the

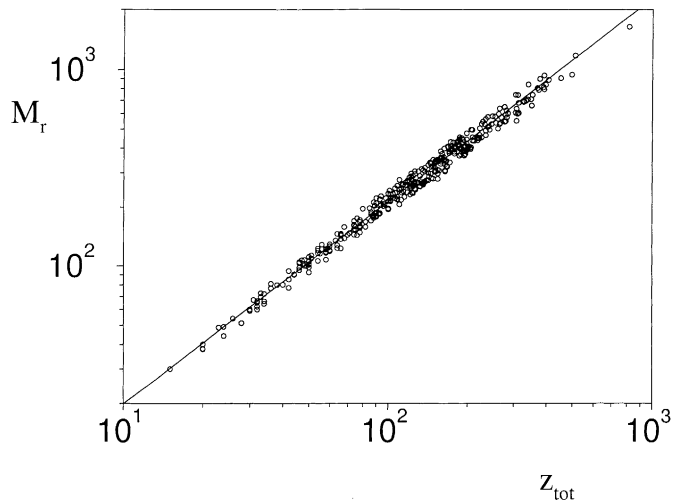

Fig. 6. Log–log M_r, Z_{tot}-plot of data points in dependence on the total proton number Z_{tot} (open circles) for the set of molecules from Table 1.

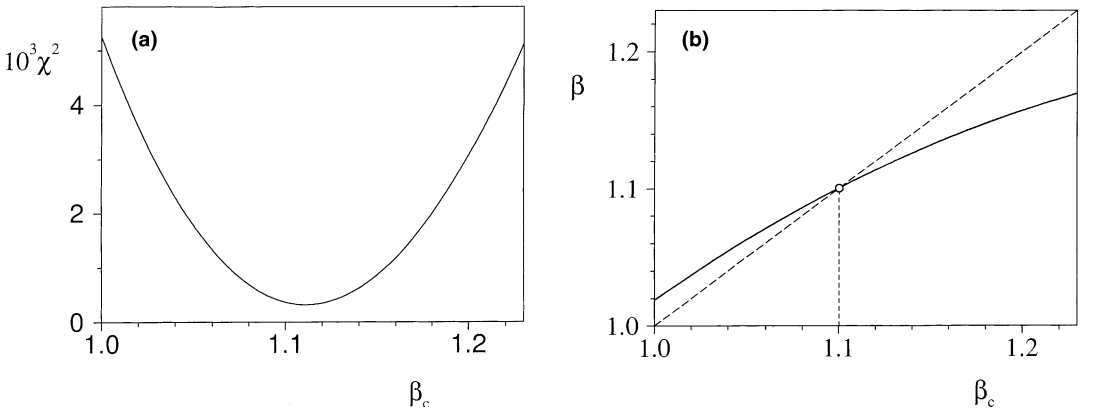

Fig. 7. Test of fit of the power law (12) for the M_r vs. Z_{eff} diagrams constructed for Z_{eff}-values corresponding to a set of uniformly distributed initial values of β_c. For each initial value of β_c the corresponding Z_{eff} value was calculated using Eq. (13). (a) χ^2-value in dependence on the initial value β_c. (b) Fitted values of β in dependence on the initial values of β_c.

power law (12) is performed to the data points in each of these diagrams. For each initial value of β_c the fitted value of β and the corresponding χ^2-value were determined. Fig. 7(a) displays χ^2 and Fig. 7(b) the power law exponent β in dependence on initial values of β_c. As seen, the best fit is obtained for $\beta_c \approx 1.1$ (Fig. 7(a)), in accordance with 14, 15.

The molecular power law (12) holds only for a finite scaling window. More stringent, the semi-empirical model of nuclei is not a very good fit for light nuclei. Thus, one can expect that the power law would be less appropriate for molecules consisting of very light nuclei only. This is seen by an analysis comparing deviations of atomic weights from the atomic power law formula for chemical elements.

In the log–log plot the χ^2-value for deviation of the atomic power law (7) from data for all stable elements is $\chi^2 = 0.004$, while excluding the five lightest elements from the fit a sizably lower χ^2-value of 0.0005 was obtained, i.e., a sizably better fit.

As a further example, the log–log plot for molecular weights M_r is presented for two sets of polymers, $(CH_2CH_2)_n$ and $(CH_2CHCl)_n$ $(n = 1, 2, 3, \ldots)$, in dependence on Z_{eff} (Fig. 8) and Z_{tot} (Fig. 9).

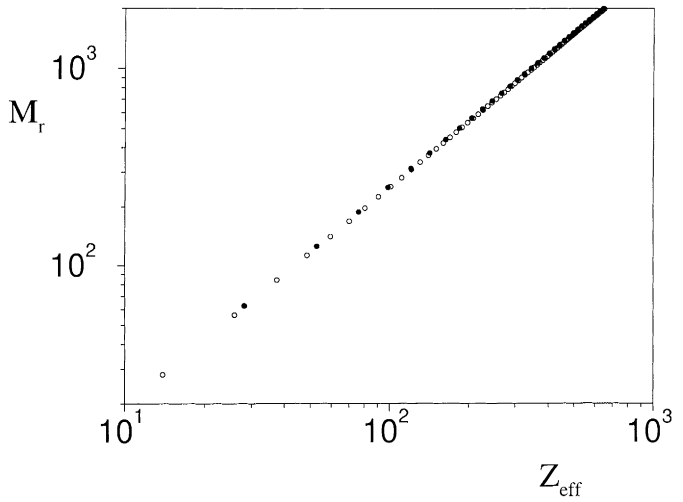

Fig. 8. Log–log M_r, Z_{eff}-plot of data points for molecular weights of organic polymers $(CH_2CH_2)_n$ and $(CH_2CHCl)_n$ $(n = 1, 2, 3, \ldots)$, in dependence on the effective molecular number Z_{eff} (open and closed circles, respectively).

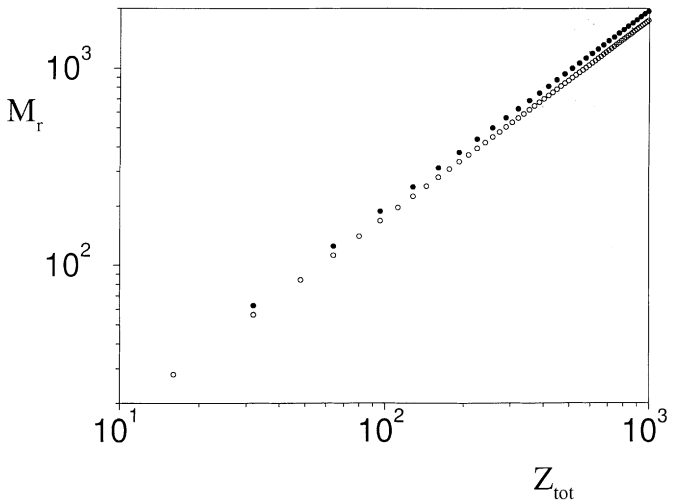

Fig. 9. Log–log M_r, Z_{tot}-plot of data points for molecular weights of organic polymers $(CH_2CH_2)_n$ and $(CH_2CHCl)_n$ ($n = 1, 2, 3, \ldots,$) in dependence on the total number of protons Z_{tot} (open and closed circles, respectively).

6. Fractality of molecular isotopic abundance set

The isotopic composition of a chemical compound (10) is obtained by taking into account that each chemical element E_i, occurring in the molecule, is composed of t_i different stable isotopes. Therefore it follows that the number of different isotopic configurations associated with the molecule (10) is

$$N = \prod_i \binom{t_i + n_i - 1}{n_i}, \tag{16}$$

where ( ) denotes the binomial coefficient.

Already for small molecules the total number of isotopic configurations is sizable. For example, for Sb_2Se_3 ($n_1 = 2$, $t_1 = 2$; $n_2 = 3$, $t_2 = 6$) Eq. (16) gives $N = 168$ isotopic configurations. For a more complex molecule $Nd(C_{11}H_{12}H_2O)_6(ClO_4)_3$ the total number of different isotopic configurations is $N = 1\ 302\ 788\ 200$.

The isotopic abundance of each isotopic configuration in a chemical compound is calculated by multiplying isotopic abundances of constituent nuclides. For example, the isotopic abundance of the isotopic configuration $^{121}Sb^{123}Sb^{78}Se^{80}Se^{80}Se$ of the chemical compound Sb_2Se_3 is $0.573 \times 0.427 \times 0.235 \times 0.496 \times 0.496 = 0.014$.

To each chemical compound (10) we assign a set of corresponding isotopic abundances (isotopic abundance set). Let us display these values along the coordinate axis. We find that this set of abundances is fractal for each chemical compound. Its fractal dimension is calculated by using the box-counting method. As an illustration, in Fig. 10 we display the $\log N_i$ vs. $\log(1/\varepsilon_i)$ diagram for the molecule Sb_2Se_3. This set is approximately fractal over a range of more than two orders of magnitude. The calculated fractal dimension is $d_f \approx 0.4$, clearly revealing its fractal nature. In the case of uniformly or randomly distributed set of points on the coordinate axis, the calculated dimension should be 1, corresponding to the absence of fractal geometry.

Displaying isotopic abundance sets of different compounds, a combined set is obtained with an overall fractal dimension. This situation could be formally compared, for example, with determination of fractal dimension of the families of asteroids, where the fractal dimension of size distribution was calculated for some asteroid families and on the basis of the cumulative size distributions an overall fractal dimension was obtained [42].

7. Mathematical model for truncated fractals

All naturally existing fractals show several fundamental differences from standard mathematical fractals: natural fractals are only approximately fractal, they extend only over a finite range of scales (having both a maximum scale and a minimum scale) and exhibit statistical fluctuations in any measure of fractal geometry. The same is true for fractals discussed in this study.

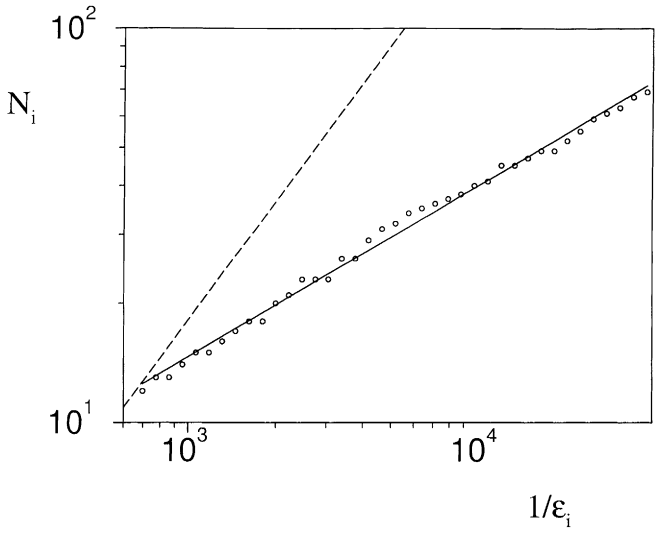

Fig. 10. Log–log plot for the number of nonempty boxes N_i vs. $1/\varepsilon_i$ (ε_i is the size of a grid box) overlaying the set of points displaying isotopic composition of the chemical compound Sb_2Se_3 along the coordinate axis. The straight line is fitted through the points calculated at several values of the box size ε_i and corresponds to the fractal dimension of 0.4. For comparison, the line corresponding to dimension of 1 is presented (dashed line).

It was recently pointed out that the scaling range of experimentally observed fractals is extremely limited, spanning roughly between 0.5 and 2.0 decades (factors of 10), while the exact fractals obey power laws over all scales [38]. On this basis it might be questionable if natural objects with a power law of limited range are indeed fractals. On the other hand, regardless of that, the result of resolution analysis is often a very useful power law, which condenses the description of a complex fractal geometry and allows one to correlate in a simple way properties of a system to its structure [38].

Here we present a discussion which could contribute to the understanding of the question whether one can claim fractal geometry of natural objects by comparing phenomenological evidence over a limited range to mathematical fractals. This is interesting for truncated fractals studied in this paper, but the same argument can be used more generally for any type of natural fractals.

In this context it should be noted that solutions of difference and differential equations for dynamical problems can also lead to fractals which are truncated and statistical, resembling the pattern of natural fractals.

One of the most prominent consequences of nonattracting chaotic sets is the phenomenon of fractal basin boundaries [68–71]. The closure of a set of initial conditions which approach a given attractor is the basin of attraction corresponding to this attractor. The boundary separating the regions belonging to different basins of attraction is referred to as the basin boundary. It is well known that the basin boundary can be fractal [68,69].

Here we address the problem whether a fractal basin boundary can be truncated, i.e., whether there is a lower cutoff at which self-similarity stops.

To this end we extend the well-known two-dimensional map on the annulus

$$\begin{aligned} \theta_{n+1} &= \theta_n + a\sin 2\theta_n - b\sin 4\theta_n - x_n\sin\theta_n, \\ x_{n+1} &= -J_0\cos\theta_n \end{aligned} \tag{17}$$

whose fractal basin boundaries were studied in [68,69]. For parameters $J_0 = 0.3$, $a = 1.32$, and $b = 0.90$ the only attractors are the fixed points $(\theta, x) = (0, -J_0)$ and (π, J_0). Computer generated pictures of the corresponding basins of attraction have revealed the Cantor set structure of the basin boundary, i.e., an infinitely fine scaled structure.

In order to induce truncation in sequences of self-similarity at a certain scale we introduce in this article a new map by extending the map (17) treating parameters a and b as dynamical quantities a_n, b_n ($n = 0, 1, 2, \ldots$) as follows. In the first four steps the values of a_n, b_n are 1.32 and 0.90, respectively, in accordance with [68,69], corresponding to the chaotic regime. For all the later steps ($n \geqslant 4$) the values of a_n, b_n are 0 and 0.2, respectively, corresponding to the regular regime. Thus, we have induced a sudden jump from chaotic into regular regime.

Thus, our extended map on the annulus reads:

$$\begin{aligned}
&\theta_{n+1} = \theta_n + a_n \sin 2\theta_n - b_n \sin 4\theta_n - x_n \sin\theta_n,\\
&x_{n+1} = -J_0 \cos\theta_n,\\
&a_n = 1.32, \quad n = 0,1,2,3,\\
&a_n = 0, \quad n \geqslant 4,\\
&b_n = 0.90, \quad n = 0,1,2,3,\\
&b_n = 0.20, \quad n \geqslant 4.
\end{aligned} \tag{18}$$

The map (18) has three coexisting attracting fixed points. Two of them, $(\theta, x) = (0, -J_0)$ and (π, J_0) for $|1 + 2a - 4b| < 1$, are the same as for the map (17). In addition, the map (18) has the third attractor at the position $(\frac{\pi}{2}, 0)$. Each of these three attractors has the corresponding basin of attraction. These three basins are displayed in Fig. 11(a). The basins are intertwined and the fractal nature of the basin boundary is revealed.

At the level of accuracy of the grid used the basin boundaries appear fractal, similarly as for the map (17), but the pattern is more complicated due to the presence of the third basin.

Let us now investigate whether this basin boundary has a Cantor set nature as in the case of map (17). From a successively magnified detail of basin boundaries in Fig. 11(b) and (c), it is seen that the basin boundaries, although having a fractal-like pattern at the scale used in Fig. 11(a), do not exhibit a Cantor set structure on finer scales. Instead, the self-similarity stops at a certain level of magnification. Thus, instead of infinitely fine scaled structure found

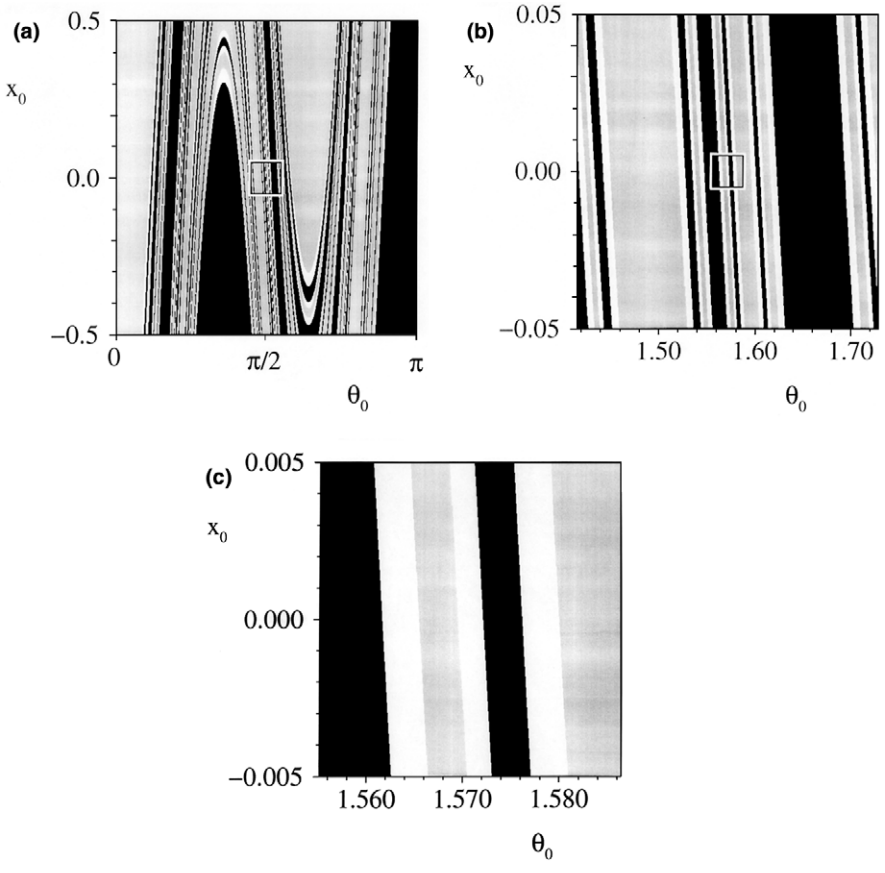

Fig. 11. (a) Basins of attraction for three attractors of the extended map (18). This figure is constructed using a 500×500 grid of initial conditions for (θ, x). Each initial condition is iterated until reaching the neighborhood of one of the attractors. If an orbit goes to the attractor at (π, J_0) a black dot is plotted at the corresponding initial condition. If the orbit goes to the attractor at $(\frac{\pi}{2}, 0)$ a blank space is left at the position of the corresponding initial condition. If the orbit goes to the attractor at $(0, -J_0)$ a gray dot is plotted. Thus, the black, gray and blank regions are pictures of the basins of attractions associated with three attractors to the accuracy of the grid used. (b) Magnification of the rectangular region in (a). (c) Magnification of the rectangular region in (b).

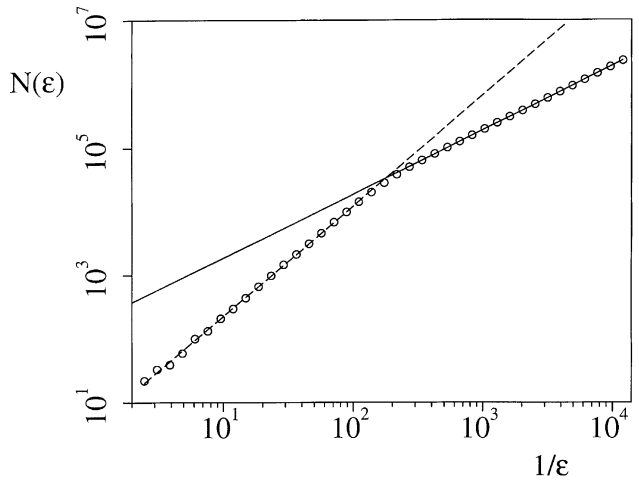

Fig. 12. Effect of truncation of fractal basin boundaries in Fig. 11 on the log–log plot for the box-counting method. For description see the text.

previously for the system (17), with fractals being self-similar at all scales [68,69], for the new system (18) we obtain truncated fractal structure for the basin boundaries, i.e., the self-similarity of fractal basin boundary stops at some critical scale. This feature of a mathematical fractal closely resembles the pattern of natural fractals, which are statistically self-similar only above some lower cutoff.

Let us note the connection of these truncated fractals for the map (18) to the previously found truncated fractals in two cases of models described by differential equations. For the sinusoidally forced pendulum modified by introduction of an additional exponential factor, so that the nonautonomous driving term decays exponentially to zero, truncated fractals were obtained [72,73]. On the other hand, in the case of a single-well Duffing oscillator it was found that the truncated fractal Arnold tongues are finely intermingled with infinitely self-similar fractal Arnold tongues, showing that a phenomenon of fractal truncation is possible in the case where the external forcing does not decrease with time [74]. It can be shown that the truncation of a fractal structure is associated with cutoff of the scaling law [75,76].

To provide an additional insight into truncated fractal in Fig. 11, we apply the box-counting method to the pattern of basin boundaries in Fig. 11. In Fig. 12 we display the number of nonempty boxes on a grid overlaid over these basin boundaries as a function of $1/\varepsilon$ (ε is the box size). It is clearly seen that a clearcut phase transition takes place at a certain value of ε, referred to as the critical value ε_c, from the fractal pattern below $1/\varepsilon_c$ (dashed line corresponding to fractal dimension of 1.7) to the nonfractal pattern above $1/\varepsilon_c$ (solid line corresponding to fractal dimension of 1.0). The critical value of box size ε_c can be related to the finest strips in Fig. 11(c), reflecting truncation of the fractal from below.

8. Conclusion

In this paper we have introduced the power law for the line of stability of atomic nuclei, for atomic weights and for molecular weights and displayed evidence for fractality of the valley of stability in nuclear chart, and of the isotopic abundances of chemical compounds.

For almost seventy years the line of stability of atomic nuclei has been described on the basis of models employing dynamics which captures some important parts of dynamics in the nuclear system. In this framework the semi-empirical mass formula appears to be a cornerstone to understand nuclear stability. In this paper an alternative approach has been adopted, based on fractal nature which appears to be present at the basic quantum mechanical level. In its quality of fitting data the power law formulated in this framework for the line of stability is comparable to the semi-microscopic formula with respect to reproducing data. Extended to most stable super-heavy nuclei, the power law corresponds to a small effective decrease of neutron excess in comparison to the semi-microscopic formula, bringing the theoretical prediction closer to the super-heavy island of stability around $Z = 114$, $N = 184$.

The power law for atomic weights arises as a consequence of fractal properties for atomic nuclei. The power law for molecular weights employs the power law for atomic weights and the new concept of the fractal-type effective molecular number Z_{eff}.

One may ask whether the molecular power law can be traced back to the power law of nuclei. Because of small electron energies, the molecular power law is determined by isotopic composition of molecules. However, one should note its close resemblance to the laws governing critical properties of assemblies of molecules.

Another point with regard to fractal geometry of natural objects is the question of the dynamics which creates the fractal character. In connection to the origin of power laws and fractal geometry introduced in this paper, it should be noted that the fractal geometry has a role in quantum physics and quark dynamics, as shown in [35]. On this basis one could expect the appearance of scale invariance at the nuclear, atomic and molecular levels.

Finally, we have presented a mathematical model which could contribute to elucidate the general problem of deducing fractal geometry of natural objects by comparing phenomenological evidence over a limited range to mathematical fractals.

References

[1] Mandelbrot BB. The fractal geometry of nature. San Francisco, CA: Freeman; 1982.
[2] Avnir D, editor. The fractal approach to heterogeneous chemistry. Chichester: Wiley; 1989.
[3] Gouyet JF. Physics and fractal structures. Paris: Masson; 1996.
[4] Turcotte DL. Fractals and chaos in geology and geophysics. Cambridge: Cambridge University Press; 1997.
[5] Bunde A, Havlin S, editors. Fractals in science. Berlin: Springer; 1995.
[6] West BJ, Deering W. Fractal physiology for physicists: Levy statistics. Phys Rep 1994;246:1–100.
[7] Bassingthwaighte JB, Liebovitch LS, West BJ. Fractal physiology. New York: Oxford University Press; 1994.
[8] Durrer R, Labini FS. A fractal galaxy distribution in a homogeneous universe? Astron Astrophys 1998;339:85–8.
[9] Pietronero L, Labini FS. Fractal universe. Physica A 2000;280:125–30.
[10] Olami Z, Feder HJ, Christensen K. Self-organized criticality in a continuous, nonconservative cellular automaton modeling earthquakes. Phys Rev Lett 1992;68:1244–7.
[11] Inaoka H, Takayasu H. Water erosion as a fractal growth process. Phys Rev E 1993;47:899–910.
[12] Radlinski AP, Radlinska EZ, Agamalian M, Wignall GD, Lindner P, Randl OG. Fractal geometry of rocks. Phys Rev Lett 1999;82:3078–81.
[13] Goetze T, Brickman J. Self-similarity of protein surfaces. Biophys J 1992;61:109–19.
[14] Goldberger AL, Bhargava V, West BJ, Mandell AJ. Nonlinear dynamics of the heartbeat. Physica D 1985;17:207–14.
[15] Lowen SB, Liebovitch LS, White JA. Fractal ion-channel behavior generates fractal firing patterns in neuronal models. Phys Rev E 1999;59:5970–80.
[16] Sernetz M, Gelleri B, Hofmann J. The organism as bioreactor. Interpretation of the reduction law of metabolism in terms of heterogeneous catalysis and fractal structure. J Theor Biol 1985;117:209–30.
[17] Krivandin AV, Muranov KO. A comparative small-angle X-ray scattering study of crystallin supramolecular structure in carp, frog and rat lenses. Biofizika 1999;44:1088–93.
[18] Braithwaite GJC, Luckham PF. Effect of molecular weight on the interactions between poly(ethylene oxide) layers adsorbed to glass surfaces. J Chem Soc Faraday Trans 1997;93:1409–15.
[19] Lobkovsky A, Gentges S, Li H, Morse D, Witten TA. Scaling properties of stretching ridges in a crumpled elastic sheet. Science 1999;270:1482–5.
[20] von Weizsäcker CF. Zur Theorie der Kernmassen. Z Physik 1935;96:431–58.
[21] Bethe HA, Bacher RF. Nuclear physics. A. Stationary states of nuclei. Rev Mod Phys 1936;8:82–229.
[22] Bohr A, Mottelson BR. In: Nuclear structure, vol. I. New York: Benjamin; 1969.
[23] Myers WD, Swiatecky WJ. Nuclear masses and deformations. Nucl Phys 1966;81:1–60.
[24] Meldner H. Predictions of new magic regions and masses for super-heavy nuclei from calculations with realistic shell model single particle Hamiltonians. Arkiv Fysik 1967;36:593–8.
[25] Mosel U, Greiner W. On the stability of superheavy nuclei against fission. Z Phys A 1969;222:261–82.
[26] Nilsson SG, Tsang CF, Sobiczewski A, Szymansky Z, Wycech S, Gustafson C, et al. On the nuclear structure and stability of heavy and superheavy elements. Nucl Phys A 1969;131:1–66.
[27] Swiatecki WJ. Nuclear physics – macroscopic aspects. Nucl Phys A 1994;574:233–51.
[28] Möller P, Nix JR. Stability and decay of nuclei at the end of the periodic system. Nucl Phys A 1992;549:84–102.
[29] Möller P, Nix JR, Myers WD, Swiatecki WJ. Nuclear ground-state masses and deformations. At Data Nucl Data Tables 1995;59:185–381.
[30] Rutz K, Bender M, Buvenich T, Schilling T, Reinhard P-G, Maruhn JA, et al. Superheavy nuclei in self-consistent nuclear calculations. Phys Rev C 1997;56:238–43.
[31] Hofmann S. Superheavy elements. Nucl Phys A 1999;654:252–69.
[32] Oganessian YT, Yeremin AV, Popeko AG, Bogomolov SL, Buklanov GV, Chelnokov ML, et al. Synthesis of nuclei of the superheavy element 114 in reactions induced by ^{48}Ca. Nature 1999;400:242–5.
[33] Ninov V, Gregorich KE, Loveland W, Ghiorso A, Hoffman DC, Lee DM, et al. Observation of superheavy nuclei produced in the reaction of ^{86}Kr with ^{208}Pb. Phys Rev Lett 1999;83:1104–7.

[34] Rowley N. Charting the shores of nuclear stability of heavy and superheavy nuclei. Nature 1999;400:209–11.
[35] Kröger H. Fractal geometry in quantum mechanics, field theory and spin systems. Phys Rep 2000;323:81–181.
[36] Walker FW, Kirouac GJ, Rourke FM. Chart of the nuclides. San Jose, CA: General Electric Company; 1977.
[37] Caserta F et al. Physical mechanisms underlying neurite outgrowth: a quantitative analysis of neuronal shape. Phys Rev Lett 1990;64:95–8.
[38] Avnir D, Biham O, Lidar D, Malcai O. Is the geometry of nature fractal? Science 1998;279:39–40.
[39] Coplen TB, Peiser HS. History of the recommended atomic-weight values from 1882 to 1997: A comparison of differences from current values to the estimated uncertainties of earlier values. Pure Appl Chem 1998;70:237–57.
[40] IUPAC 1997. Standard atomic weights. www.webelements.com.
[41] Mills I, Cvitaš T, Hofmann K, Kallay N, Kuchitsu K. Quantities, units and symbols in physical chemistry. London: Blackwell; 1993.
[42] Zaninetti L, Cellino A, Zappala V. On the fractal dimension of the families of asteroids. Astron Astrophys 1995;294:270–3.
[43] Rubčić A, Rubčić J, Arp H. New empirical clues for the factor 1.23. In: Redshift, electromagnetism, cosmology: Toward a new synthesis. Montreal: Apeiron; 2001.
[44] Tang S, McFarlane CM, Paul GC, Thomas CR. Characterising latex particles and fractal aggregates using image analysis. Colloid Polymer Sci 1999;277:325–33.
[45] Vincze A, Fata R, Zrinyi M, Horvolgyi Z, Kertesz J. Comparison of aggregation of rodlike and spherical particles – A fractal analysis. J Chem Phys 1997;107:7451–8.
[46] Earnshaw JC, Robinson DJ. Inter-cluster scaling in two-dimensional colloidal aggregation. Physica A 1995;214:23–51.
[47] Meakin PA. A historical introduction to computer models for fractal aggregates. J Sol–Gel Sci Tecnol 1999;15:97–117.
[48] Kyriakidis AS, Yiantsios SG, Karabelas AJ. A study of colloidal particle Brownian aggregation by light scattering techniques. J Colloid Interface Sci 1997;195:299–306.
[49] Cameron C, Fawcett AH, Hetherington CR, Mee RAW, Mcbride FV. Cycles frustrating fractal formation in an AB(2) step growth polymerization. Chem Commun 1997;18:1801–2.
[50] Rogovina LZ, Slonimskii GL. Structure and properties of critical gels. Vysokomol Soedin Ser A 1997;39:1543–56.
[51] Haw MD, Poon WCK, Pusey PN. Structure and arrangement of clusters in cluster aggregation. Phys Rev A 1997;56:1918–33.
[52] Valsami G, Macheras P. Determination of fractal reaction dimension in dissolution studies. Eur J Pharmaceutical Sci 1995;3:163–9.
[53] Daoud M. Polymers. In: Bunde A, Havlin S, editors. Fractals in science. Berlin: Springer; 1995. p. 163–95.
[54] Avnir D, Gutfraind R, Farin D. Fractal analysis in heterogeneous chemistry. In: Bunde A, Havlin S, editors. Fractals in science. Berlin: Springer; 1995. p. 229–55.
[55] Tanaka S, Itoh S, Kurita N. Structural and vibrational analysis of azodendrimers by molecular orbital methods. Chem Phys Lett 2000;323:407–15.
[56] Lecomte A, Dauger A, Lenormand P. Dynamical scaling property of colloidal aggregation in a zirconia-based precursor sol during gelation. J Appl Crystallogr 2000;33:496–9.
[57] Sorensen CM, Wang GM. Size distribution effect on the power law regime of the structure factor of fractal aggregates. Phys Rev E 1999;60:7143–8.
[58] Winter R, Gabke A, Czeslik C, Pfeifer P. Power-law fluctuations in phase-separated lipid membranes. Phys Rev E 1999;60:7354–9.
[59] Ikeda S, Foegeding EA, Hagiwara T. Rheological study on the fractal nature of the protein gel structure. Langmuir 1999;15:8584–9.
[60] Lavallee C, Berker A. More on the prediction of molecular weight distributions of linear polymers from their rheology. J Rheol 1997;41:851–71.
[61] Jin HW, Jin CQ. Fractal surfaces of 8-(hydroxyquinoline)zinc and their relation to electroluminescence behaviour. Polym Polym Compos 2000;8:263–6.
[62] Ogasawara T, Izawa K, Hattori N, Okabayashi H, O'Connor CJ. Growth process for fractal polymer aggregates formed by perfluorooctyltrimethoxysilane. Time-resolved small-angle X-ray scattering study. Colloid Polym Sci 2000;278:293–300.
[63] Provata A, Almirantis Y. Cantor patterns in the sequence structure of DNA. Fractals 2000;8:15–27.
[64] Kirchner JW, Feng XH, Neal C. Fractal stream chemistry and its implications for contaminant transport in catchments. Nature 2000;403:524–7.
[65] Kolesnikov YL, Sechkarev AV, Zemskii VI. Fractal dynamics of molecules in new composite optical materials. J Opt Technol 2000;67:360–4.
[66] Paar V, Pavin N, Rubčić A, Rubčić J, Trinajstić N. Scale invariant power law and fractality for molecular weights. Chem Phys Lett 2001;336:129–34.
[67] Weast RC, editor. Handbook of chemistry and physics. Cleveland, OH: Chemical Rubber Co.; 1968.
[68] Grebogi C, Ott E, Yorke JA. Final state sensitivity: an obstruction to predictability. Phys Lett A 1983;99:415–8.
[69] McDonald SW, Grebogi C, Ott E, Yorke JA. Fractal basin boundaries. Physica D 1985;17:125–53.
[70] Grebogi C, Kostelich E, Ott E, Yorke JA. Multi-dimensioned intertwined basin boundaries: basin structure of the kicked double rotor. Physica D 1987;25:347–60.
[71] Ott E. Chaos in dynamical systems. Cambridge: Cambridge University Press; 1993.
[72] Varghese M, Thorp JS. Truncated-fractal basin boundaries in forced pendulum systems. Phys Rev Lett 1988;60:665–8.
[73] Dobson I, Delchamps DF. Truncated fractal basin boundaries in the pendulum with nonperiodic forcing. J Nonlinear Sci 1994;4:315–28.

[74] Paar V, Pavin N. Intermingled fractal Arnold tongues. Phys Rev E 1998;57:1544–9.
[75] Paar V, Pavin N, Truncated fractal basin boundaries and cutoff of uncertainty exponent for extended map on annulus, unpublished.
[76] Paar V, Pavin N, Rosandic M. Link between truncated fractals and coupled oscillators in biological systems. J Theor Biol 2001;212:47–56.